Title: GASOTRANSMITTER MODULATION OF HYPOGLOSSAL MOTONEURON ACTIVITY

Abbreviated Title: Heme Oxygenase and Hypoglossal Motoneurons

Authorship: Brigitte Browe[1,2,3], Ying-Jie Peng[1], Jayasri Nanduri[1,3], Nanduri R. Prabhakar[1,2,3], Alfredo J. Garcia III[1,2,3]

Affiliations:

[1]Institute for Integrative Physiology, The University of Chicago; [2]Grossman Institute for Neuroscience, Quantitative Biology & Human Behavior, The University of Chicago.
[3]Department of Medicine, Section of Emergency Medicine, The University of Chicago.

Keywords: hydrogen sulfide, heme oxygenase 2, hypoglossal motor nucleus, inspiratory drive

Authors Contribution: Experimental design by AJG, NRP, and BB. Experiments and analyses performed by BB, AJG, SK and JN. BB wrote the first draft. BB, AJG, and NRP revised and edited the manuscript.

Correspondence: Alfredo Garcia: ajgarcia3@uchicago.edu

Figure Number: 8

Table Number: 0

Introduction: 385

Abstract: 177

Significance Statement:

Discussion: 641

Acknowledgements:

Funding Sources:

This work was supported by NIH P01 HL144454 (NRP) and NIH R01NS107421 (AJG).

Abstract

Obstructive sleep apnea (OSA) is characterized by periodic disruption of breathing due to sporadic collapse of upper airway. Mice with targeted deletion of the gene *Hmox2,* encoding the enzyme heme oxygenase-2 (HO-2), exhibit severe OSA. Upper airway patency is governed by genioglossal nerve activity originating from the hypoglossal motor nucleus. We tested the hypothesis that disrupted HO-2 signaling weakens hypoglossal motoneuron activity using a combination of genetic, biochemical and electrophysiological approaches. Hypoglossal neurons are positive for HO-2. Disrupting HO-2 function caused transmission failure of inspiratory rhythm from preBötzinger complex (preBötC) to the hypoglossal nucleus. Failed transmission coincided with smaller inspiratory drive currents and a reduced intrinsic excitability among hypoglossal neurons. Hypoglossal neurons also expressed cystathionine □-lyase (CSE), an H_2S producing enzyme. H_2S abundance was higher in hypoglossal neurons of HO-2 null mice than wild-type controls. Disrupting CSE function normalized transmission from preBötC to hypoglossal neurons in HO-2 null mice. An H_2S donor mimicked the effects of disrupted HO-2 function in wild type mice. These findings demonstrate a hitherto uncharacterized modulation of hypoglossal motoneurons by HO-2 and CSE-derived H_2S.

Introduction

Obstructive sleep apnea (OSA) is a prevalent breathing disorder affecting nearly a billion people throughout the world [1],[2]. OSA is characterized by periodic cessation of breathing during sleep due to sporadic collapse of upper airway, and untreated OSA predisposes to a variety of diseases including hypertension [3],[4], diabetes[5],[6], and cognitive decline [7],[8]. Multiple factors contribute to genesis of OSA including compromised pharyngeal anatomy [9] [10], inadequate upper airway muscle function [11],[12],[13], low arousal threshold [14], and a hypersensitive chemoreflex (i.e., high loop gain [15]), arising in part from the carotid body, the principal sensory organ for monitoring arterial blood O_2 levels.

We recently reported mice with deletion of the *Hmox 2* gene, which encodes the enzyme hemeoxygenase 2 (HO-2), exhibit high incidence of OSA [16]. OSA in HO-2 null mice was attributed, in part, to the increased loop gain arising from the heightened carotid body chemo reflex [16],[17],[18],[19]. However, whether HO-2 signaling by direct action in the central nervous system also contribute to OSA has not been examined.

Upper airway patency is maintained by genioglossal nerve activity originating from the hypoglossal nucleus. Sporadic loss of airway patency during OSA is due to periodic reductions in genioglossal nerve activity [20, 21]. Whether impaired HO-2 signaling causes sporadic loss of hypoglossal neurons is not known. Here we tested the hypothesis, that disrupted HO-2 signaling weakens inspiratory drive originating from the hypoglossal nucleus. This possibility was tested using a combination of electrophysiological, genetic, and pharmacological approaches.

Methods

Study Approval. In accordance with National Institutes of Health guidelines, all animal protocols were performed with the approval of the Institute of Animal Care and Use Committee at The University of Chicago.

Experimental Animals. Experiments were performed on age- and body-weight–matched male and female WT (C57/BL6; Charles River) and HO-2 null mice (from S. H. Snyder; The Johns Hopkins University), HO-2 and CSE double-null mice were created by crossing HO-2 null females with CSE null males (from R. Wang, Department of Biology, Laurentian University, Sudbury, ON, Canada). Experiment involved tissues from both sexes. No sex-based differences were observed; therefore, all sexes were pooled for analysis. All litters were housed with their dam in ALAAC-approved facilities on a 12 hour / 12-hour light-dark cycle.

Pharmacological Agents. Heme oxygenase activity was blocked using bath application of Cr(III)Mesoporphyrin IX chloride (CrM459, 20μM; Frontiers Sciences, Newark DE). Fast synaptic glycinergic and GABAergic inhibition was blocked by bath application of strychnine (1μM; Sigma), and pictrotoxin (PTX; 45μM; Sigma), respectively. Inhibition of CSE production was accomplished by *in vivo* L-propargylglycine (L-PAG, 30mg/kg (Sigma, St. Louis MO) administered (*i.p.* injection) 2.5 to 3 hrs prior to preparation of the rhythmic brainstem slice preparation.

Measurement of H_2S Production. Coronal brainstem sections (300μm thick) were cut with a cryostat at –20°C. XIIn and control brainstem regions were excised with a chilled micro-punch needle. H_2S levels in the micro punches pooled from 2 mice were determined as described previously [22]. Briefly, cell homogenates were prepared in 100 mM potassium phosphate buffer (pH 7.4). The enzyme reaction was carried out in sealed tubes. The assay mixture in a total volume of 500μL contained (in final concentration): 100 mM potassium phosphate buffer

(pH 7.4), 800μM L-cysteine, 80μM pyridoxal 5′-phosphate with or without L-PAG (20μM) and cell homogenate (20μg of protein) The reaction mixture was incubated at 37°C for 1 h. At the end of the reaction, alkaline zinc acetate (1% wt/vol; 250μL) and trichloroacetic acid (10% vol/vol) were sequentially added to trap H_2S and stop the reaction, respectively. The zinc sulfide formed was reacted with acidic N,N-dimethyl-p-phenylenediamine sulfate (20μM) and ferric chloride (30μM) and the absorbance was measured at 670 nm using Shimadzu UV-VIS Spectrophotometer. L-PAG inhibitable H_2S concentration was calculated from a standard curve and values are expressed as nanomoles of H_2S formed per hour per mg of protein.

Immunohistochemistry. Anaesthetized mice (urethane, 1.2g•kg^{-1} *i.p.*) were perfused transcardially with heparinized phosphate-buffered saline (PBS) for 20 min followed by 4% paraformaldehyde in PBS. Brainstems were harvested, post-fixed in 4% paraformaldehyde overnight, and cryoprotected in 30% sucrose/PBS at 4°C. Frozen tissues were serially sectioned at a thickness of 20μm (coronal section) and stored at –80°C. Sections were treated with 20% normal goat serum, 0.1% bovine serum albumin and 0.1% Triton X-100 in PBS for 30 min and incubated with primary antibodies against choline acetyltransferase (ChAT, 1:100; Millipore; #AB144P), HO-2 (1:200, Novus Biologicals; # NBP1-52849) and CSE (1:250; gift from Dr. Schenider) followed by Texas Red-conjugated goat anti-mouse IgG or FITC-conjugated goat anti-rabbit IgG (1/250; Molecular Probes). After rinsing with PBS, sections were mounted in Vecta shield containing DAPI (Vector Labs) and analyzed using a fluorescent microscope (Eclipse E600; Nikon).

Brainstem Slice for Electrophysiology. The isolated rhythmic brainstem slice was prepared as previously described [23]. Briefly, animals were euthanized by decapitation. Brainstems were rapidly dissected, isolated, and placed into ice cold aCSF (in mM: 118 NaCl, 25 $NaHCO_3$, 1 NaH_2PO_4, 1 $MgCl_2$, 3 KCl, 30 Glucose, 1.5 $CaCl_2$, pH=7.4) equilibrated with 95% O_2, 5% CO_2. The isolated brainstem was glued to an agar block (dorsal face to agar) with the rostral face up

and submerged in ACSF equilibrated with carbogen. Serial cuts were made through the brainstem until the appearance of anatomical landmarks such as the narrowing of the fourth ventricle and the hypoglossal axons. The preBötC and XIIn was retained in a single transverse brainstem slice (thickness: 560 ± 40µm). The slice was retained and transferred into the recording chamber (~6mL volume) where it was continuously superfused (12 -15mL/min) with recirculating aCSF. Prior to recording, extracellular KCl was raised to 8mM and the spontaneous rhythm allowed to stabilize prior to the start of every experiment.

Electrophysiology. Extracellular population activity was recorded with glass suction pipettes filled with ACSF were positioned over the ventral respiratory column containing the preBötC and a second pipette positioned over the medial dorsal column containing the hypoglossal nucleus recorded the transmission of the preBötC population activity. In some experiments, a third pipette was position between the preBötC and hypoglossal nucleus just lateral to the axon tract to record intermediate transmission through the premotor field containing intermediate premotor inspiratory neurons [24, 25]. Extracellular population activity was recorded with glass suction pipettes filled with aCSF [26]. The recorded signal was sampled at 5kHz, amplified 10,000X, with a lowpass filter of 10 kHz using an A-M instruments (A-M Systems, Sequim, WA, USA) extracellular amplifier. The signal was then rectified and integrated using Clampfit electronic filter. Recordings were stored on a computer for *posthoc* analysis.

All recordings intracellular recordings were made using the Multiclamp 700B (Molecular Devices: https://www.moleculardevices.com/systems/conventional-patch-clamp/multiclamp-700b-microelectrode-amplifier). Acquisition and post hoc analyses were performed using the Axon pCLAMP10 software suite (Molecular Devices: https: www.moleculardevices.com/system/axon-conventional-patch-clamp/pclamp-11-software-suite).

Whole cell patch clamp recordings of hypoglossal motor neurons were obtained using the blind-patch technique with a sample frequency of 40 kHz. Recordings were made with unpolished

patch electrodes, pulled from borosilicated glass pipettes with a capillary filament [26]. The electrodes had a resistance of 4-6.5 MΩ when filled with the whole cell patch clamp pipette solution containing (in mM): 140 K-gluc acid, 1 $CaCl_2$, 10 EGTA, 2 $MgCl_2$, 4 Na_2-ATP, 10 HEPES. Patch clamp experiments were performed with a patch clamp amplifier (Multipatch 700B, Molecular Devices, Sunnyvale, CA, USA), and the software program pCLAMP 10.0 (Molecular Devices). Neurons located at least two to three cell layers (about 75-250µm) rostral from the caudal surface of the slice were recorded. Neurons located directly at the slice surface were not examined because their dendritic processes were more likely to be damaged during the preparation than those of neurons located deeper within the slice. The liquid junction potential was calculated to be -12mV and was subtracted from the membrane potential. The series resistance was compensated and corrected throughout each experiment. In voltage clamp experiments, membrane potential was held at -60mV. Current clamp experiments used a holding potential between 0 and -100pA to establish the baseline resting membrane potential between -55 and -70mV.

***Statistical Analyses*.** All n values are total number of animals, unless otherwise stated. Transmission was expressed as a percentage of the hypoglossal network bursts corresponding to the total network bursts from either the preBötC or the premotor field. Input: Output (I/O) ratios were calculated similar to previously described in by Garcia et al. [26]. preBötC bursts without a corresponding XIIn burst were designated as 0. The mean I/O value for each experimental condition was calculated in each slice. Statistics were performed using Origin 8 Pro (OriginLab, RRID:SCR_014212) or Prism 6 (GraphPad Software; RRID:SCR_015807). Comparisons between two groups were conducted using either paired or unpaired two-tailed t-tests with Welch's correction, where appropriate. A one-way ANOVA was performed followed by *posthoc* Dunnett's test comparing experimental groups to control when a comparison of three or

more groups. Results are presented as the mean ± S.E.M. Differences were defined when the P-value was less than 0.05.

Results

Hypoglossal neurons express hemeoxygenase-2 (HO-2). We first assessed whether hypoglossal neurons express HO-2 using immunohistochemical approaches. Hypoglossal neurons showed positive expression for HO-2 as indicated by co-localization with ChAT, an established marker of these neurons [11] (**Fig.1A**).

Disrupting HO-2 function impairs hypoglossal inspiratory activity. Extracellular field recordings in the rhythmic brainstem slice were simultaneously recorded from the preBötC and the corresponding inspiratory motor output from the hypoglossal nucleus. Two approaches were employed to assess the role of HO-2: (1) using Cr(III) Mesoporphyrin IX chloride (ChrMP459, 20µM), an inhibitor of HO [27]; and (2) using brain slices from HO-2 null mice.

Examples of extracellular field recordings from the preBötC and hypoglossal nucleus prior and during ChrMP459 exposure were shown in **Fig 1B**). While ChrMP459 suppressed hypoglossal burst amplitude (**Fig 1C**, *left*), the HO inhibitor had no effect on preBötC burst amplitude (**Fig 1C**, *right*)**.** The reduced hypoglossal burst amplitude was also associated with failed transmission of inspiratory drive from preBötC to the hypoglossal nucleus (**Fig 2D).** Impaired transmission can reflect an altered input-output relationship between preBötC and the hypoglossal nucleus [26]. Therefore, the I/O ratio between the preBötC and the hypoglossal nucleus were compared during baseline and with ChrMP459. The HO inhibitor reduced the I/O ratio (**Fig 1E)**, suggesting that ChrMP 459 leads to a generalized weakening of I/O relationship between preBötC and hypoglossal motoneurons.

ChrMP459 is a pan HO inhibitor, which cannot distinguish between heme oxygenase isoforms HO-1 and HO-2. To assess the specific contribution of HO-2, studies were performed using brainstem slices from HO-2 null mice. Brainstem slices from wild type controls showed 100% transmission of inspiratory drive from preBötC to the hypoglossal nucleus **(Fig. 2A-B**); whereas brain slices from HO-2 null mice displayed deficits in transmission (**Fig 2 A-B**). The impaired transmission coincided with a smaller I/O ratio (**Fig 2C).** These findings established

that disrupted HO-2 function leads to reduced transmission from inspiratory preBötC to hypoglossal neurons. Given that the effects of ChrMP 459 were similar to HO-2 null mice and the limited availability of HO-2 null mice, the following studies were performed using HO-inhibitor.

HO inhibitor does not affect premotor neuron activity. Intermediary premotor neurons relay inspiratory drive from the preBötC to the hypoglossal nucleus [24, 25]. Therefore, it was possible that HO inhibition impaired transmission of inspiratory drive from preBötC by perturbing inspiratory activity from intermediary premotor neurons. To address this possibility, triple extracellular recordings were made from the preBötC, the field of the ipsilateral premotor neurons, and the hypoglossal nucleus. Baseline transmission from preBötC to the premotor field and to the hypoglossal nucleus was reliable and consistent (**Fig. 3A,** *middle panel*). However, ChrMP459 disrupted inspiratory activity in the hypoglossal nucleus despite unaltered activities in either preBötC or the intermediate premotor field (**Fig 3A**, *right panel*). Indeed, while neither transmission of inspiratory drive nor I/O ratio from preBötC to the premotor field was affected by ChrMP459 (**Fig 3B**), the HO inhibitor did reduce transmission of inspiratory drive and I/O ratio metrics between the premotor field and the hypoglossal nucleus (**Fig 3C**). These results indicated HO-2 modulates postsynaptic activity of the hypoglossal nucleus.

HO inhibition suppresses inspiratory drive currents and excitability in hypoglossal neurons. To address the effect of HO inhibitor on postsynaptic activity of the hypoglossal neurons, patch clamp recordings were made from hypoglossal neurons receiving inspiratory drive. We focused on the impact of ChrMP459 on inspiratory-related fast glutamatergic synaptic drive by application of picrotoxin and strychnine to eliminate confounding effects from fast synaptic inhibition (**Fig 4A**). Peak inspiratory drive currents were reduced in presence of ChrMP459 (**Fig 4B-C**). Moreover, disinhibited hypoglossal neurons showed a wide range of rheobase values. Under baseline conditions, 6 of the 12 neurons studied exhibited a rheobase less than 100pA (range11-75 pA); whereas the other neurons had a rheobase value >100pA

(range 195-492 pA). ChrMP459 increased rheobase in hypoglossal neurons with lower baseline rheobase (<100pA) and tended to decrease rheobase with a baseline rheobase greater than 100pA (**Fig 4E).** Consequently, we recorded in current clamp configuration to further examine the impact of HO inhibitor on excitability of hypoglossal neurons ChrMP459 suppressed excitability of spontaneously firing of hypoglossal neurons (**Fig. 5A-B**) as indicated by reduced number of action potentials during the preBötC burst activity (**Fig 5C).** These findings indicated that the HO inhibitor reduces rhythmic drive and suppress intrinsic excitability of hypoglossal neurons.

HO-2 null mice manifest elevated H_2S abundance in the hypoglossal nucleus. We next sought to determine the mechanism(s) by which inhibition of HO-2 affect hypoglossal neuron activity. Earlier studies reported that HO-2 null mice manifest increased H_2S production from CSE in the peripheral [28] and central [29] nervous system, suggesting that HO-2 is a negative regulator of H_2S production. We hypothesized that activation of CSE and the ensuing increased H_2S production affect hypoglossal neuronal activity. To test this possibility, we first examined whether the hypoglossal neurons express CSE. Brainstem sections from the WT hypoglossal nucleus revealed CSE expression in ChAT-positive neurons (**Fig 6A**). We then determined H_2S abundance in hypoglossal tissue punches from WT and HO-2 null mice. Relative to the WT hypoglossal nucleus (**Fig 6B** *blue*), H_2S abundance was greater in the hypoglossal nucleus of HO-2 null mice (**Fig 6B** *red*), but not different from the inferior olive brainstem region of HO-2 null mice (**Fig 6B** *grey*). These findings demonstrated that the hypoglossal nucleus expresses CSE and HO-2 negatively regulatesH_2S production in the hypoglossal nucleus.

H_2S mediates impaired transmission of inspiratory drive caused by disrupted HO-2 function. If the impaired transmission of inspiratory drive to the hypoglossal nucleus by disrupted HO-2 function involves CSE-derived H_2S then: 1) a H_2S donor should mimic the effects of disrupted HO-2 activity, and 2) CSE blockade should restore the transmission from preBötC to the hypoglossal nucleus. The following experiments tested these possibilities.

WT brainstem slices manifested a nearly 1:1 ratio (100 ± 0.73%) of transmission of inspiratory activity from preBötC to hypoglossal neurons (**Fig 6C**, left). Application of NaHS, a H_2S donor reduced transmission from preBötC to hypoglossal (**Fig. 6C,** middle, right) in a dose-dependent manner (**Fig. 6D,** 50μM, 100μM), which coincided with a reduction in I/O ratio by NaHS (**Fig.6E**). These findings demonstrated increased H_2S abundance reduces hypoglossal neuronal activity consistent with findings using either ChrM459 or HO-2 null mice. Thus, the stability of inspiratory transmission from the preBötC to hypoglossal nucleus appear to be negatively affected either by increasing H_2S abundance or by disrupting HO-2 function.

Given that CSE produces H_2S, we first used HO-2:CSE double null mice to determine how genetic ablation of CSE impacted inspiratory activity in the brainstem slice from HO-2 null mice. Simultaneous extracellular field recordings of inspiratory activity from the preBötC and hypoglossal neurons of HO-2:CSE double null mice revealed near absence of failed transmission (**Fig 7A-B**, n=6) and a larger I/O ratio (**Fig 7C**) when compared to data from HO-2 null mice.

To further assess the role of CSE, we treated HO-2 null mice with L-PAG, an inhibitor of CSE. Indeed, L-PAG treatment improved transmission of inspiratory activity to the hypoglossal nucleus (**Fig. 8A-B,** left) and restored the I/O ratio compared to untreated HO-2 null mice (**Fig. 8B,** right). Moreover, intermittent transmission failure was also evident in patch clamp recordings from untreated HO-2 null hypoglossal neurons (**Fig 8C**, *left*) but not in HO-2 null hypoglossal neurons treated with L-PAG (**Fig. 8C**, *right*). These reduced transmission events also correlated with smaller individual inspiratory drive currents in HO-2 null hypoglossal neurons when compared to corresponding inspiratory drive currents from L-PAG treated HO-2 mice (**Fig. 8D-E**). These genetic and pharmacological experiments implicated the impaired inspiratory activity caused by disrupted HO-2 signaling in hypoglossal neurons involve CSE-dependent H_2S signaling.

Discussion

Based on the earlier report that HO-2 null mice exhibit high incidence of OSA [16], current study determined whether HO-2 deficient mice manifest intact hypoglossal neuron function, which maintain upper airway patency. Our results demonstrated that: 1) hypoglossal neurons express HO-2; 2) perturbing HO-2 function impairs transmission of inspiratory drive from the preBötC to the hypoglossal nucleus, which was due to altered postsynaptic properties; 3) hypoglossal neurons are also positive for CSE, a H_2S producing enzyme; 4) H_2S abundance was greater in the hypoglossal nucleus of HO-2 null mice than WT controls; 5) Blocking CSE function in HO-2 mice normalized the transmission of from the preBötC to the hypoglossal neurons; and 6) An H_2S donor, like HO-2 null mice, impaired transmission at hypoglossal neurons. These findings reveal a hitherto uncharacterized modulation of hypoglossal neuron function by HO-2 and CSE-derived H_2S.

Consistent with an earlier report [30], we also found hypoglossal neurons were positive for HO-2, and further showed that these neurons indeed belong to hypoglossal nucleus as evidenced by HO-2 co-localization with ChAT. The neurophysiological significance of HO-2 was assessed in a brainstem slice preparation, with intact transmission of inspiratory activity originating from the preBötC to hypoglossal neurons. Our results showed that a pharmacological inhibitor of HO-2 impaired transmission of neural drive from preBötC to hypoglossal neurons and this effect appear to be not due to non-specific action of HO inhibitor as similar results were also obtained using HO-2 null mice.

Mice treated with intermittent hypoxia (IH) patterned after blood O_2 profiles seen during OSA also show failed transmission between preBötC and hypoglossal nucleus [26],[31]. However, IH-induced impaired transmission was associated with alterations in preBötC activity, whereas the HO inhibitor had no effect on inspiratory rhythmogenesis from the preBötC (**Fig. 1C**). Moreover, the HO inhibitor did not perturb transmission of the neuronal drive to intermediate premotor neurons suggesting that impaired interneuron function was not a major

contributing factor to the impaired transmission observed in the hypoglossal nucleus. These findings suggested that HO inhibition impairs neuronal transmission by directly affecting the intrinsic excitability of hypoglossal nucleus. This possibility was supported by patch clamp studies showing decreased neural drive current, an increased rheobase, and reduction of action potentials generated per neural burst in hypoglossal neurons.

How might disrupted HO-2 function affect hypoglossal neuron function? Hypoglossal neurons expressed CSE, an H_2S producing enzyme, and HO-2 null mice showed increased abundance of H_2S in hypoglossal neurons, suggesting HO-2 is a negative regulator of CSE derived H_2S production as reported elsewhere in the peripheral and central nervous system [28], [29]. Electrophysiological experiments demonstrated that an H_2S donor produced both failed transmission of inspiratory drive to the hypoglossal nucleus and reduced the I/O ratio—phenomena similar to that observed when perturbing HO-2 activity. Additionally, genetic ablation of CSE improved transmission of inspiratory drive the hypoglossal nucleus in HO-2 null mice. A CSE inhibitor, L-PAG, in HO-2 null mice also restored transmission from preBötC to the hypoglossal nucleus and increased inspiratory drive currents in hypoglossal neurons.

Cystathionone β-synthase (CBS) is another H_2S producing enzyme which is expressed throughout the CNS, primarily in astrocytes [32]. However, an earlier study reported that inhibition of CBS has little impact on inspiratory activity from the hypoglossal nucleus [33]. Moreover, as our patch clamp experiments used picrotoxin and strychnine, the effects of CSE-derived H_2S appear to be independent of changes to fast inhibitory drive. H_2S appears to weaken the inspiratory drive currents as well as reducing intrinsic excitability of hypoglossal neurons.

How might enhanced H_2S signaling reduce drive currents, and excitability of hypoglossal neurons? While it is possible that H_2S may directly impact presynaptic release of glutamate and/or postsynaptic receptor activity of hypoglossal neurons, the increase in rheobase observed in some neurons in HO inhibitor treated slices implicates potential involvement of a non-synaptic

conductance as a downstream effector of H_2S based signaling arising from perturbed HO-2 activity. ATP-sensitive K^+ channel (K_{ATP}) activity has been shown to be increased by H_2S in several cell types including cerebral arterioles [34], and smooth muscle of the colon [35]. Microinjection of H_2S into respiratory network, especially parafacial respiratory group inhibits inspiratory discharge from hypoglossal rootlets, which can be prevented with co-administration of the K_{ATP} blocker, glibenclamide, with H_2S [36]. K_{ATP} is dynamically active in rhythmic hypoglossal neurons causing periodic adjustment of excitability of upper airway motor neurons [37]. It is likely that H_2S mediated regulation of hypoglossal neurons involve K_{ATP} channels, a possibility that remains to be established in future studies.

In conclusion, our study provides proof-of-concept for the existence of a central mechanism by which loss of HO-2 leads to reduced upper airway tone through regulation of H_2S acting in the hypoglossal nucleus. This mechanism appears to be localized to hypoglossal motoneurons involves the antagonistic relationship between HO-2 and CSE. Although OSA in HO-2 null mice was attributed to increased “loop-gain” arising from the hypersensitive carotid body reflex [16], our findings indicate potential involvement of a disrupted interaction between HO-2 and CSE-H_2S in upper airway motoneurons contributing to OSA observed in HO2 deficient mice.

Figure legends

Figure 1. Disruption of hemeoxygenase-2 (HO-2) in hypoglossal motor neurons impairs inspiratory activity from the hypoglossal nucleus but not preBötC. **A.** HO-2 (red bottom left) is expressed in $ChAT^+$ cells (green bottom right) of the hypoglossal nucleus (XIIn, combined top). **B.** Integrated traces of network activity in spontaneously rhythmic brainstem slices recorded from XIIn (grey) and preBötC (black) before (top) and after (bottom) bath application of 20µM ChrMP459 (ChrMP), failed transmission events are highlighted (pink boxes); scale bar: 5 sec. **C.** Integrated Burst Amplitude change from Baseline to ChrMP in XIIn (left) and preBötC (right). **D.** Comparison of inspiratory drive transmission in XIIn between Baseline and ChrMP. **E.** Comparison of I/O ratio of preBötC to XIIn burst size between Baseline and ChrMP (n=11).

Figure 2. Genetic deletion of HO-2 leads to uncoupling of inspiratory rhythm in the rhythmic brain slice and a reduced I/O relationship between preBötC and XIIn. A. Representative integrated traces of network burst activity in preBötC and XIIn in rhythmic slices from WT (left) and HO-2 null ($HO\text{-}2^{-/-}$, right) mice; scale bar: 2 sec. **B.** Transmission of inspiratory rhythmic activity from preBotC to XIIn in slices from WT vs HO-2 null mice. **C.** I/O ratio comparison in WT and $HO\text{-}2^{-/-}$ mice. (WT: n=8; $HO\text{-}2^{-/-}$ n=7). WT control data originally plotted in Figure 1D and 1E.

Figure 3. While ChrMP459 does not change transmission from the preBötC to the premotor area, ChrMP459 increases transmission failure from the premotor area to the XIIn. A. Diagram of medullary brain slice showing XIIn (light grey, 1), premotor field (dark grey, 2), and preBötC (black, 3) and corresponding representative traces of integrated network activity in Baseline (left) and in 20µM ChrMP (right); scale bar: 1 sec. **B.** Comparison of transmission (left) and I/O ratio (right) between preBötC to the premotor field. **C.** Comparison of transmission (left) and I/O ratio (right) between the premotor field and XIIn (n=5).

Figure 4. Heme oxygenase inhibition reduces inspiratory drive currents in XIIn neurons. **A.** Representative traces of a XIIn neuronal activity ($V_{holding}$= -60mV) aligned with corresponding integrated network activity from preBötC (∫) before (Baseline) and after 20 µM ChrMP. scale bar: 1 sec x 10pA. **B.** Magnification of highlighted (red dotted box in **A**) drive currents from Baseline and ChrMP; scale bar: 100 msec x 10pA. **C.** Comparison of XIIn inspiratory drive current magnitude in Baseline and ChrMP (n=8). **D.** Representative trace of current clamp recording in response to ramp current injection (red trace) in Baseline (grey trace) and ChrMP (black trace); scale bars: 1 sec x 40mV x 200pA. **E.** Comparison of rheobase in Baseline and ChrMP in XIIn neurons. Rheobase was divided into two groups: <100pA (left, n=6) and >100pA (right, n=6).

Figure 5. ChrMP459 reduces action potentials derived from inspiratory drive. A. Representative traces of a XIIn neuron spontaneously active with ipsilateral preBötC network bursts (∫) in Baseline and 20 µM ChrMP (skipped transmission of action potentials in ChrMP highlighted in pink); scale bar 2sec x 20mV. **B.** Magnification of highlighted (red box in **A**) XIIn bursting activity; scale bars: 100msec x 25mV. **C.** Average number of action potentials generated per inspiratory burst fired in Baseline and ChrMP bath application (n=6).

Figure 6. CSE-dependent H_2S is abundantly produced in XIIn tissue and exogenous NaHS disrupts inspiratory drive in the hypoglossal motor neuron. A. CSE (red, bottom left) is expressed in $ChAT^+$neurons (green, bottom right) in the XIIn (overlay, top). **B.** CSE-dependent H_2S generation in XIIn from WT compared to HO-$2^{-/-}$ XIIn (red area in slice diagram) and inferior olive (grey area in slice diagram). Tissue punches of XIIn and inferior olive taken at bregma between -7.20mm and -7.90mm. (WT: XIIn n=6; HO-$2^{-/-}$: XIIn n=6; inferior olive n=4). **C.** Integrated traces from XIIn (top) and preBötC (bottom) during baseline, and in response to the H2S donor, NaHS, at 50 µM and 100 µM. After NaHS application, XIIn but not preBotC burst amplitude were diminished (red dashed box) and in some cases, preBötC drive failed to produce activity in the XIIn (pink box). **D.** Comparison of transmission from preBötC to XIIn after

NaHS application at 10μM, 50μM and 100μM. **E.** I/O ratios for each NaHS concentration. (Baseline: n=9; 10μM n=5; 50μM n=6; 100μM n=9).

Figure 7. HO-2:CSE null mice do not exhibit XIIn transmission failures. A. Representative extracellular recordings from preBötC and XIIn in slices from HO-2:CSE null (HO-2:CSE$^{-/-}$); scale bar 2 sec. **B.** Transmission from preBötC to XIIn from HO-2$^{-/-}$ and HO-2:CSE$^{-/-}$ (n=6). **C.** I/O ratio from preBötC to XIIn in HO-2$^{-/-}$ and HO-2:CSE$^{-/-}$. HO-2$^{-/-}$ data replotted from Figure 2.

Figure 8. Transmission failures in HO-2 null mice are rescued with CSE inhibitor L-propargylglycine. A. Representative trace of integrated activity of the preBötC (bottom) and XIIn (top) in slices from HO-2 null mice treated with L-PAG (L-PAG). Scale bar 2 sec. **B.** Transmission (left) and I/O ratios (right) were compared between HO-2$^{-/-}$ (n=7) and L-PAG slices (n=5). **C.** Representative voltage clamp recordings of XIIn drive currents were recorded in HO-2$^{-/-}$ (n=7) and L-PAG (n=6); scale bar 10 msec x 20pA. Skipped transmission between preBötC (bottom) the XIIn neuron (top) occurs in untreated HO-2$^{-/-}$ (highlighted by pink boxes) but not in neurons from L-PAG. **D.** Magnified representative drive potentials from HO-2$^{-/-}$ and L-PAG (from highlighted by red-outlined boxes in **C**). scale bars: 100 msec x 10pA. **E.** Quantification of drive currents received by XIIn motoneurons from HO-2$^{-/-}$ mice (n=8) produce smaller drive potentials when compared to L-PAG (n=6).

Citations

1. Lyons, M.M., et al., *Global burden of sleep-disordered breathing and its implications.* Respirology, 2020. **25**(7): p. 690-702.
2. Malhotra, A., et al., *Metrics of sleep apnea severity: beyond the apnea-hypopnea index.* Sleep, 2021. **44**(7).
3. Mehra, R., *Sleep apnea and the heart.* Cleve Clin J Med, 2019. **86**(9 Suppl 1): p. 10-18.
4. Yeghiazarians, Y., et al., *Obstructive Sleep Apnea and Cardiovascular Disease: A Scientific Statement From the American Heart Association.* Circulation, 2021. **144**(3): p. e56-e67.
5. Loffler, K.A., et al., *Continuous Positive Airway Pressure Treatment, Glycemia, and Diabetes Risk in Obstructive Sleep Apnea and Comorbid Cardiovascular Disease.* Diabetes Care, 2020. **43**(8): p. 1859-1867.
6. Hua, F., *New insights into diabetes mellitus and its complications: a narrative review.* Ann Transl Med, 2020. **8**(24): p. 1689.
7. Daulatzai, M.A., *Cerebral hypoperfusion and glucose hypometabolism: Key pathophysiological modulators promote neurodegeneration, cognitive impairment, and Alzheimer's disease.* J Neurosci Res, 2017. **95**(4): p. 943-972.
8. Bibbins-Domingo, K., et al., *Screening for Obstructive Sleep Apnea in Adults: US Preventive Services Task Force Recommendation Statement.* Jama, 2017. **317**(4): p. 407-414.
9. Castro, D. and L.A. Freeman, *Oropharyngeal Airway*, in *StatPearls*. 2022, StatPearls Publishing Copyright © 2022, StatPearls Publishing LLC.: Treasure Island (FL).
10. Genta, P.R., et al., *Airflow Shape Is Associated With the Pharyngeal Structure Causing OSA.* Chest, 2017. **152**(3): p. 537-546.
11. Neelapu, B.C., et al., *Craniofacial and upper airway morphology in adult obstructive sleep apnea patients: A systematic review and meta-analysis of cephalometric studies.* Sleep Med Rev, 2017. **31**: p. 79-90.
12. Vos, W.G., W.A. De Backer, and S.L. Verhulst, *Correlation between the severity of sleep apnea and upper airway morphology in pediatric and adult patients.* Curr Opin Allergy Clin Immunol, 2010. **10**(1): p. 26-33.
13. Kubin, L., *Neural Control of the Upper Airway: Respiratory and State-Dependent Mechanisms.* Compr Physiol, 2016. **6**(4): p. 1801-1850.
14. Eckert, D.J., et al., *Defining phenotypic causes of obstructive sleep apnea. Identification of novel therapeutic targets.* Am J Respir Crit Care Med, 2013. **188**(8): p. 996-1004.
15. Nemati, S., et al., *Model-based characterization of ventilatory stability using spontaneous breathing.* J Appl Physiol (1985), 2011. **111**(1): p. 55-67.
16. Peng, Y.J., et al., *Complementary roles of gasotransmitters CO and H2S in sleep apnea.* Proc Natl Acad Sci U S A, 2017. **114**(6): p. 1413-1418.
17. Peng, Y.J., et al., *Therapeutic Targeting of the Carotid Body for Treating Sleep Apnea in a Pre-clinical Mouse Model.* Adv Exp Med Biol, 2018. **1071**: p. 109-114.
18. Osman, A.M., et al., *Obstructive sleep apnea: current perspectives.* Nat Sci Sleep, 2018. **10**: p. 21-34.
19. Prabhakar, N.R. and G.L. Semenza, *Gaseous messengers in oxygen sensing.* J Mol Med (Berl), 2012. **90**(3): p. 265-72.
20. Fleury Curado, T.A., et al., *Silencing of Hypoglossal Motoneurons Leads to Sleep Disordered Breathing in Lean Mice.* Front Neurol, 2018. **9**: p. 962.
21. Fleury Curado, T., et al., *Chemogenetic stimulation of the hypoglossal neurons improves upper airway patency.* Sci Rep, 2017. **7**: p. 44392.

22. Yuan, S., et al., *Hydrogen sulfide metabolism regulates endothelial solute barrier function.* Redox Biol, 2016. **9**: p. 157-166.
23. Garcia, A.J., 3rd, et al., *Chronic Intermittent Hypoxia Differentially Impacts Different States of Inspiratory Activity at the Level of the preBötzinger Complex.* Front Physiol, 2017. **8**: p. 571.
24. Koizumi, H., et al., *Structural-functional properties of identified excitatory and inhibitory interneurons within pre-Botzinger complex respiratory microcircuits.* J Neurosci, 2013. **33**(7): p. 2994-3009.
25. Revill, A.L., et al., *Dbx1 precursor cells are a source of inspiratory XII premotoneurons.* Elife, 2015. **4**.
26. Garcia, A.J., 3rd, et al., *Chronic Intermittent Hypoxia Alters Local Respiratory Circuit Function at the Level of the preBötzinger Complex.* Front Neurosci, 2016. **10**: p. 4.
27. Ding, Y., Y.L. Li, and H.D. Schultz, *Downregulation of carbon monoxide as well as nitric oxide contributes to peripheral chemoreflex hypersensitivity in heart failure rabbits.* J Appl Physiol (1985), 2008. **105**(1): p. 14-23.
28. Prabhakar, N.R., *Carbon monoxide (CO) and hydrogen sulfide (H(2)S) in hypoxic sensing by the carotid body.* Respir Physiol Neurobiol, 2012. **184**(2): p. 165-9.
29. Morikawa, T., et al., *Hypoxic regulation of the cerebral microcirculation is mediated by a carbon monoxide-sensitive hydrogen sulfide pathway.* Proc Natl Acad Sci U S A, 2012. **109**(4): p. 1293-8.
30. Mazza, E., et al., *Expression of heme oxygenase in the oxygen-sensing regions of the rostral ventrolateral medulla.* J Appl Physiol (1985), 2001. **91**(1): p. 379-85.
31. Zanella, S., et al., *When norepinephrine becomes a driver of breathing irregularities: how intermittent hypoxia fundamentally alters the modulatory response of the respiratory network.* J Neurosci, 2014. **34**(1): p. 36-50.
32. Enokido, Y., et al., *Cystathionine beta-synthase, a key enzyme for homocysteine metabolism, is preferentially expressed in the radial glia/astrocyte lineage of developing mouse CNS.* Faseb j, 2005. **19**(13): p. 1854-6.
33. da Silva, G.S.F., et al., *Excitatory Modulation of the preBötzinger Complex Inspiratory Rhythm Generating Network by Endogenous Hydrogen Sulfide.* Front Physiol, 2017. **8**: p. 452.
34. Liang, G.H., et al., *Hydrogen sulfide dilates cerebral arterioles by activating smooth muscle cell plasma membrane KATP channels.* Am J Physiol Heart Circ Physiol, 2011. **300**(6): p. H2088-95.
35. Gade, A.R., M. Kang, and H.I. Akbarali, *Hydrogen sulfide as an allosteric modulator of ATP-sensitive potassium channels in colonic inflammation.* Mol Pharmacol, 2013. **83**(1): p. 294-306.
36. Chen, L., et al., *K(ATP) channels of parafacial respiratory group (pFRG) neurons are involved in H2S-mediated central inhibition of respiratory rhythm in medullary slices of neonatal rats.* Brain Res, 2013. **1527**: p. 141-8.
37. Haller, M., et al., *Dynamic activation of K(ATP) channels in rhythmically active neurons.* J Physiol, 2001. **537**(Pt 1): p. 69-81.

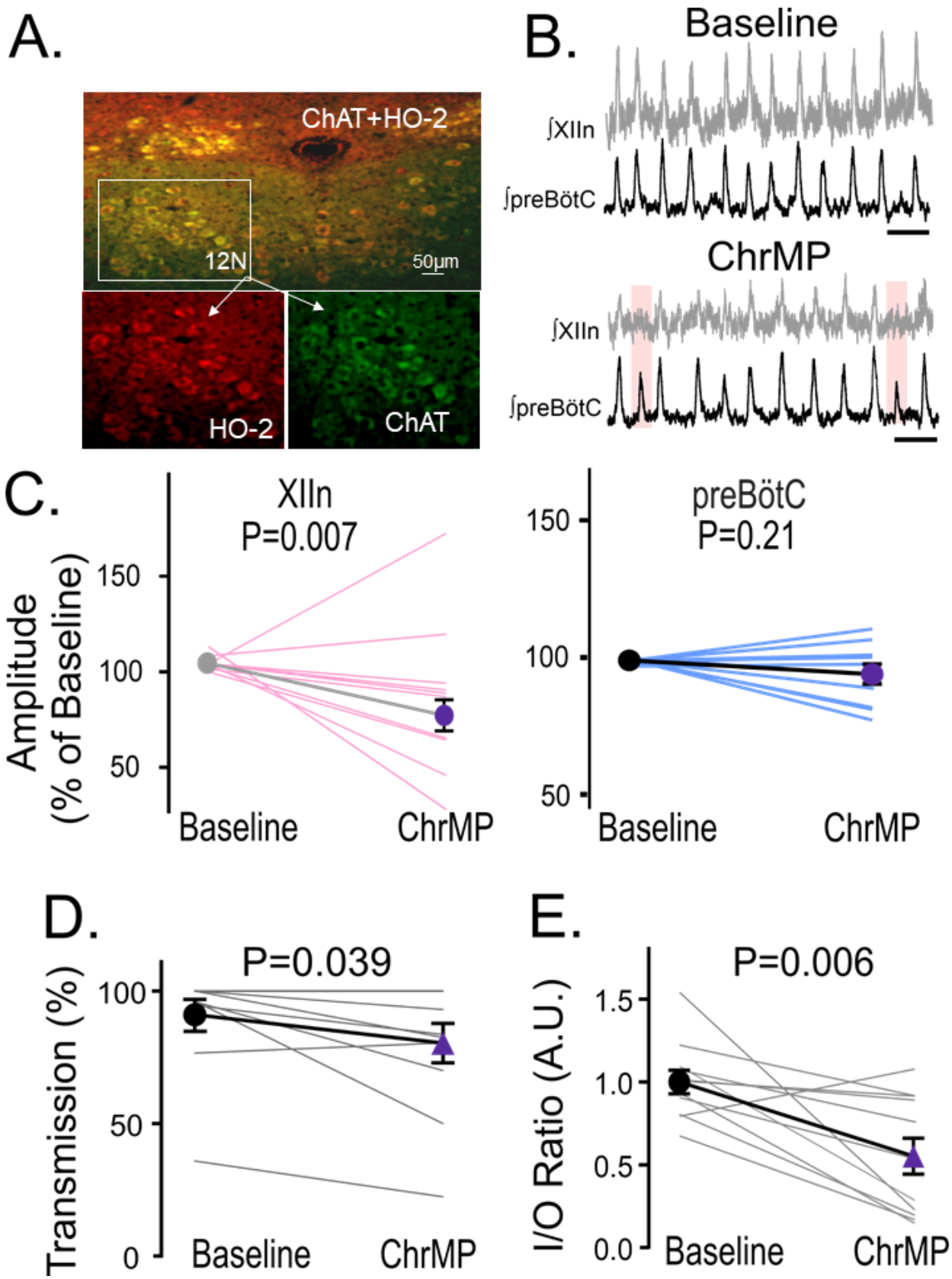
A.
ChAT+HO-2
12N
50µm
HO-2
ChAT
B.
Baseline
∫XIIn
∫preBötC
ChrMP
∫XIIn
∫preBötC
C.
XIIn
P=0.007
Amplitude
(% of Baseline)
150
100
50
Baseline
ChrMP
preBötC
P=0.21
150
100
50
Baseline
ChrMP
D.
P=0.039
Transmission (%)
100
50
0
Baseline
ChrMP
E.
P=0.006
I/O Ratio (A.U.)
1.5
1.0
0.5
0.0
Baseline
ChrMP

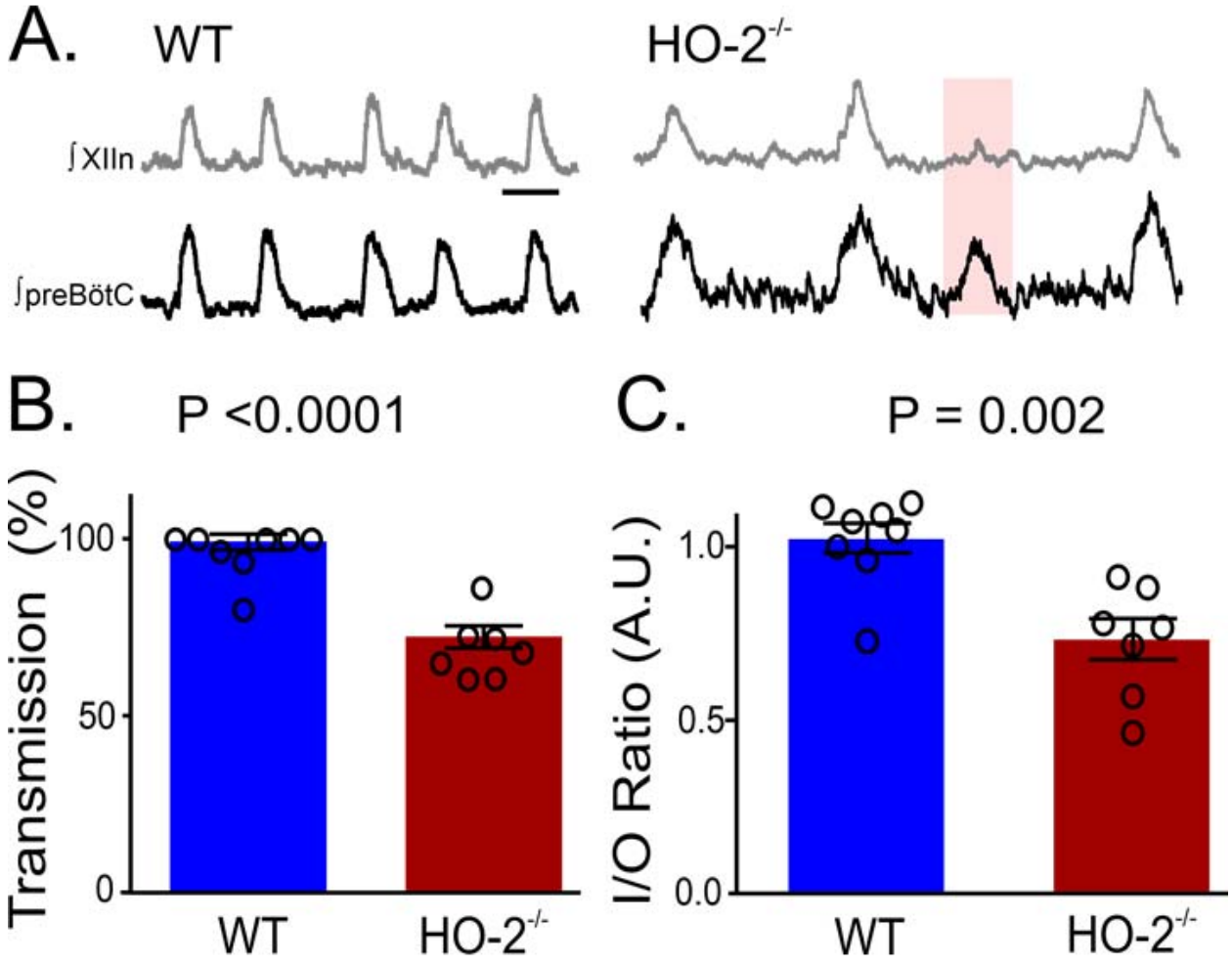
A.
WT
HO-2-/-
∫XIIn
∫preBötC
B.
P <0.0001
Transmission (%)
100
50
0
WT
HO-2-/-
C.
P = 0.002
I/O Ratio (A.U.)
1.0
0.5
0.0
WT
HO-2-/-

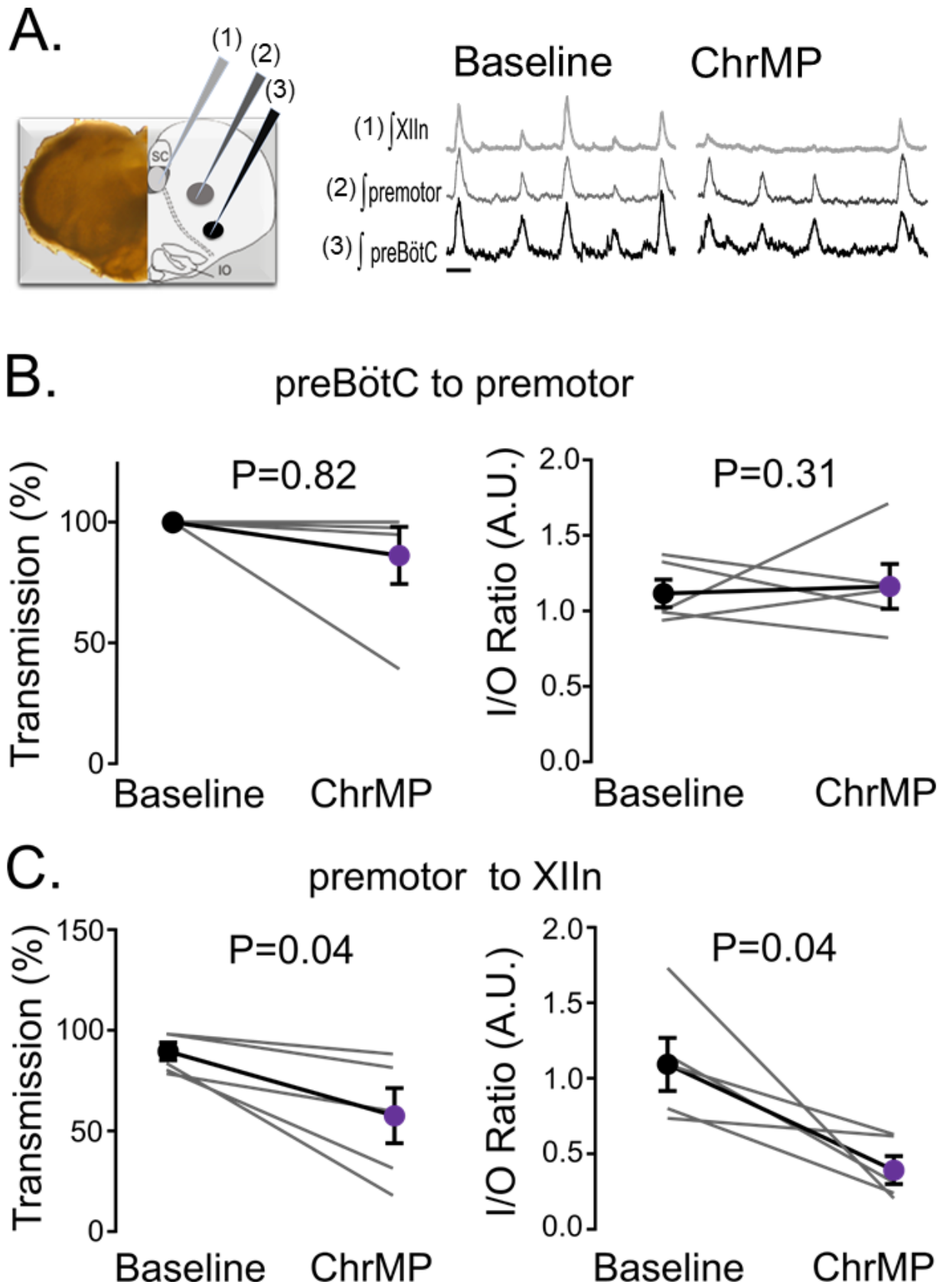
A.
(1)
(2)
(3)
SC
IO
Baseline
ChrMP
(1) ∫XIIn
(2) ∫premotor
(3) ∫ preBötC
B.
preBötC to premotor
P=0.82
Transmission (%)
100
50
0
Baseline
ChrMP
P=0.31
I/O Ratio (A.U.)
2.0
1.5
1.0
0.5
0.0
Baseline
ChrMP
C.
premotor to XIIn
P=0.04
Transmission (%)
150
100
50
0
Baseline
ChrMP
P=0.04
I/O Ratio (A.U.)
2.0
1.5
1.0
0.5
0.0
Baseline
ChrMP

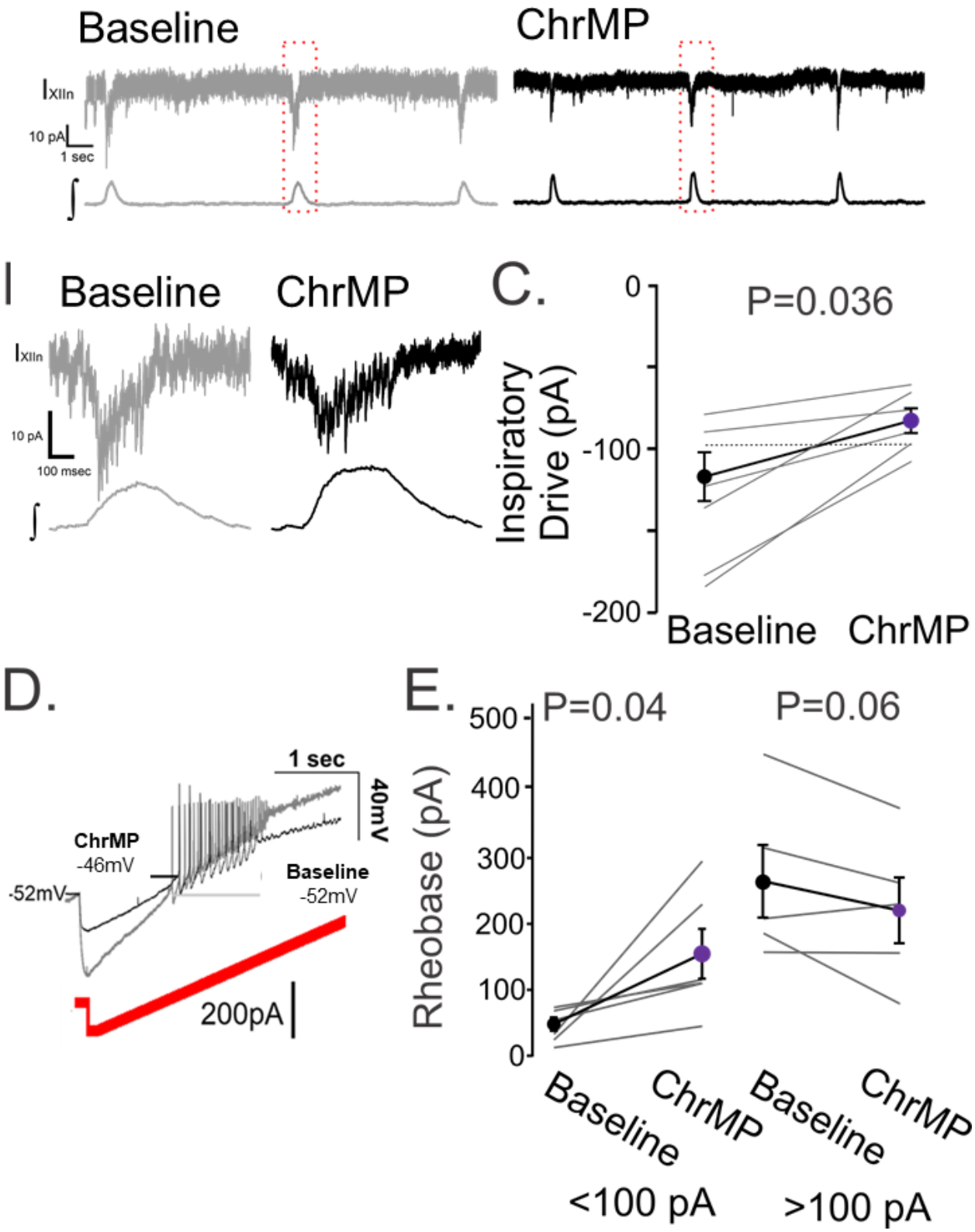
Baseline
ChrMP
IXIIn
10 pA
1 sec
I
Baseline
ChrMP
IXIIn
10 pA
100 msec
C.
P=0.036
Inspiratory Drive (pA)
0
-100
-200
Baseline
ChrMP
D.
1 sec
40mV
ChrMP
-46mV
-52mV
Baseline
-52mV
200pA
E.
P=0.04
P=0.06
Rheobase (pA)
500
400
300
200
100
0
Baseline
ChrMP
Baseline
ChrMP
<100 pA
>100 pA

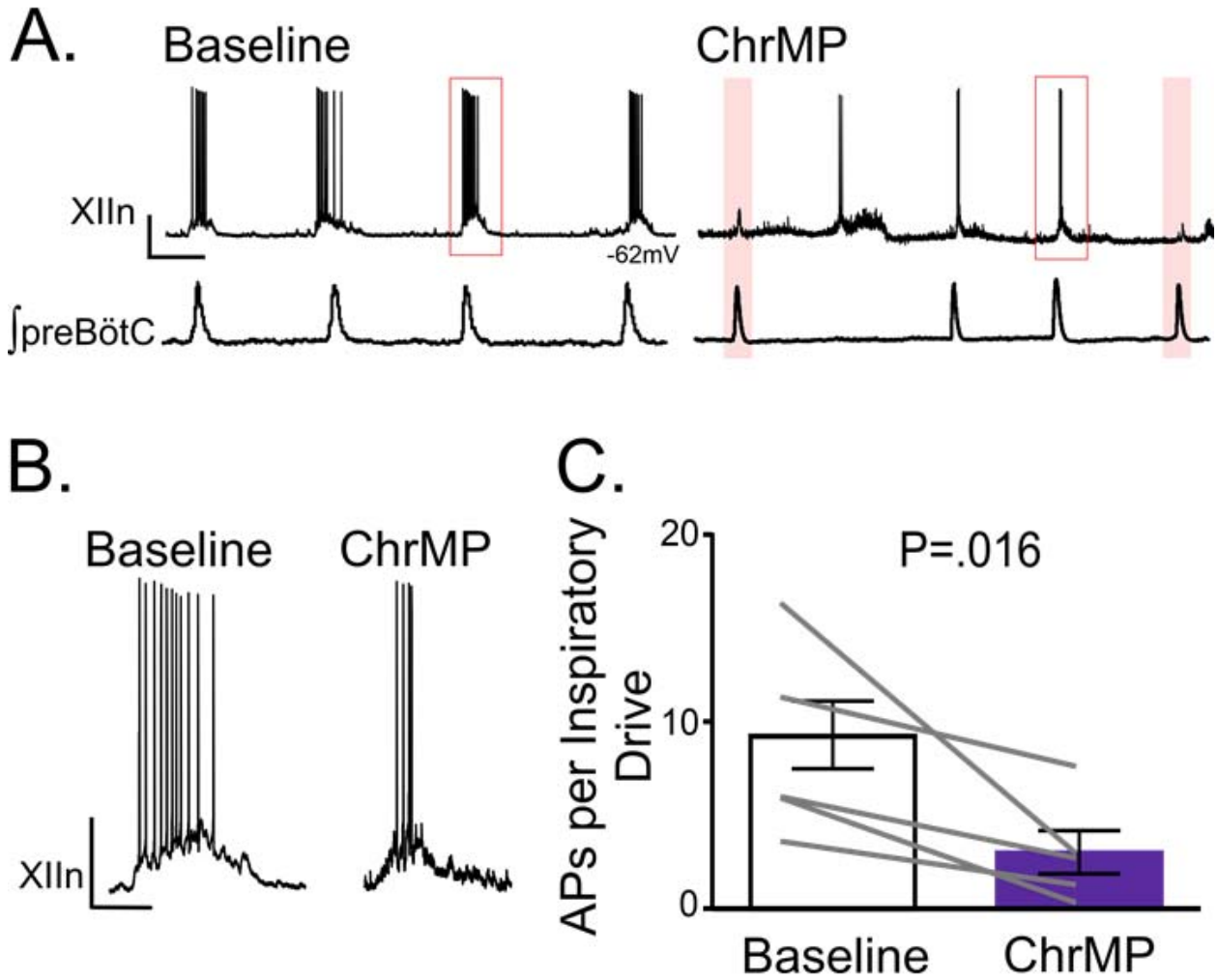
A.
Baseline
ChrMP
XIIn
-62mV
∫preBötC
B.
Baseline
ChrMP
XIIn
C.
APs per Inspiratory Drive
20
10
0
P=.016
Baseline
ChrMP

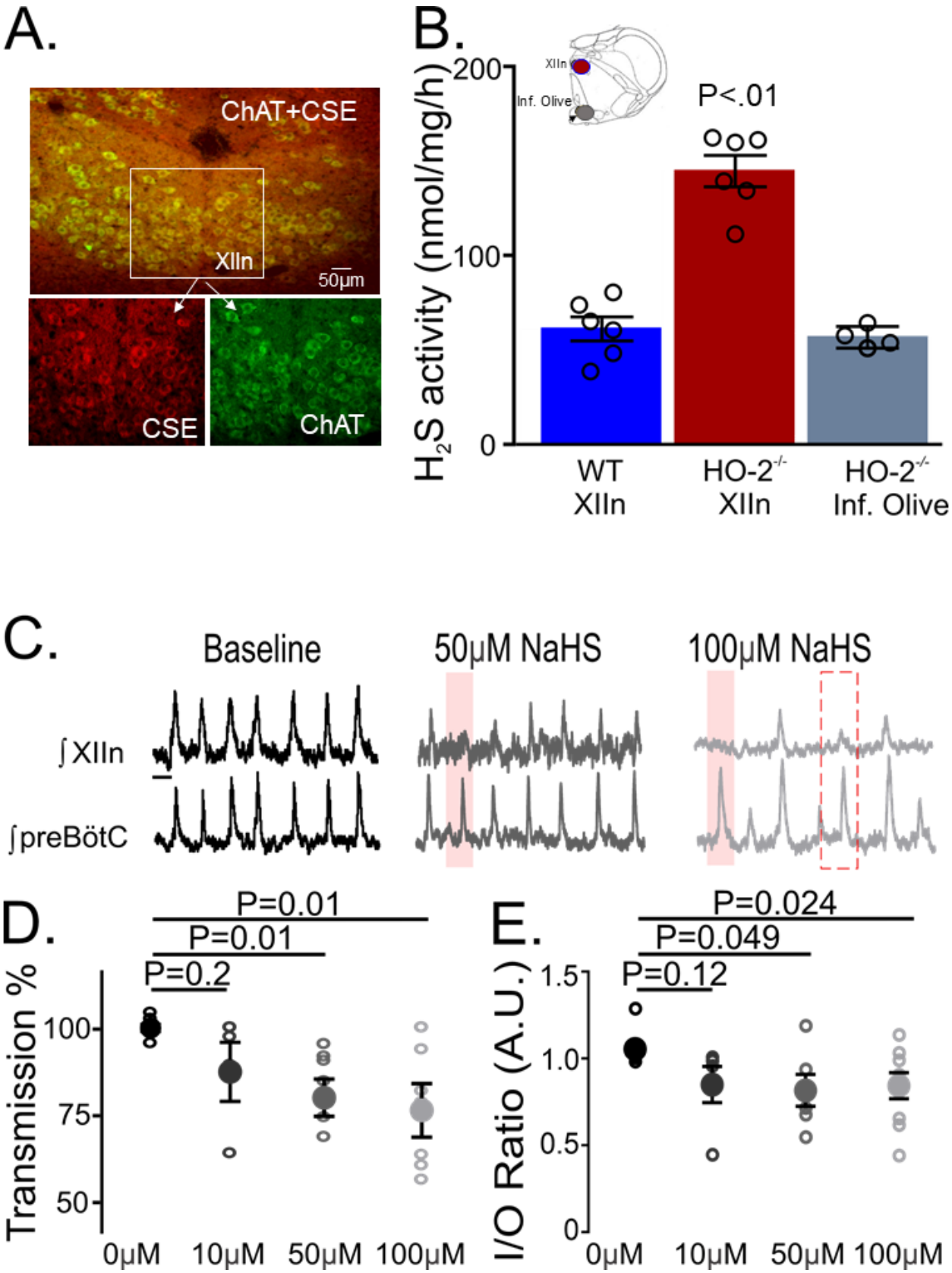
A.
ChAT+CSE
XIIn
50µm
CSE
ChAT
B.
XIIn
Inf. Olive
P<.01
H_2S activity (nmol/mg/h)
200
100
0
WT XIIn
HO-2$^{-/-}$ XIIn
HO-2$^{-/-}$ Inf. Olive
C.
Baseline
50µM NaHS
100µM NaHS
∫XIIn
∫preBötC
D.
P=0.01
P=0.01
P=0.2
Transmission %
100
75
50
0µM
10µM
50µM
100µM
E.
P=0.024
P=0.049
P=0.12
I/O Ratio (A.U.)
1.5
1.0
0.5
0
0µM
10µM
50µM
100µM

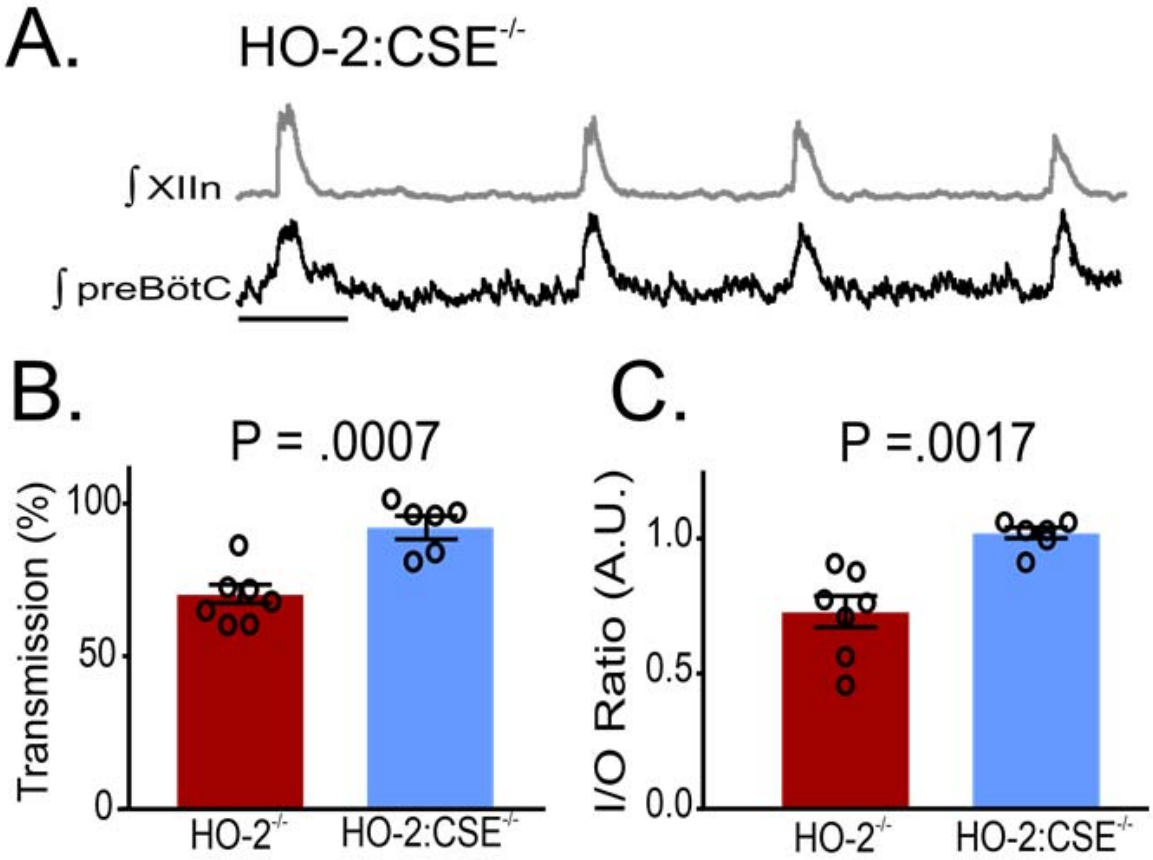
A.
HO-2:CSE-/-
∫XIIn
∫preBötC
B.
P = .0007
Transmission (%)
100
50
0
HO-2-/-
HO-2:CSE-/-
C.
P =.0017
I/O Ratio (A.U.)
1.0
0.5
0.0
HO-2-/-
HO-2:CSE-/-

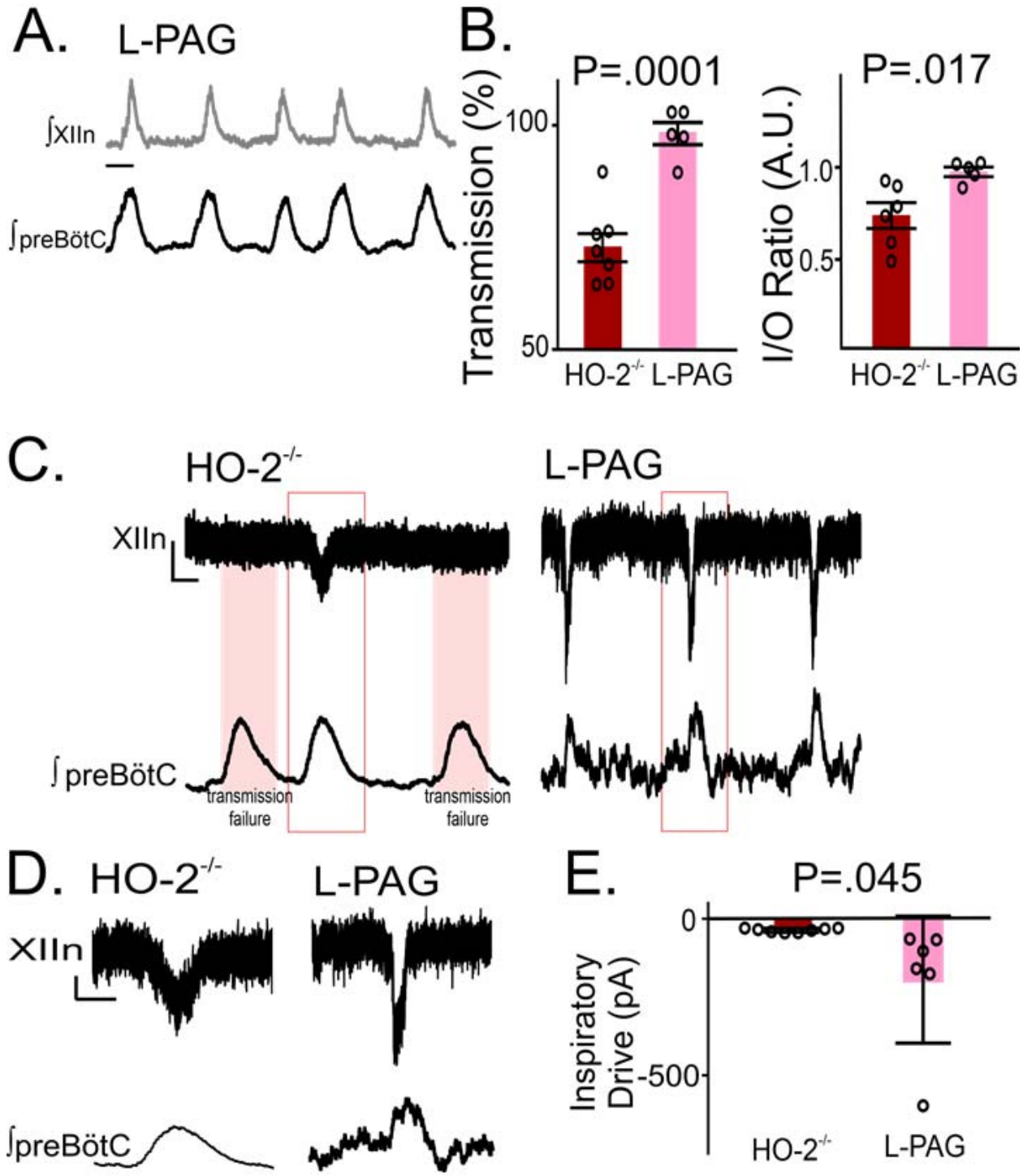
A.
L-PAG
∫XIIn
∫preBötC
B.
P=.0001
Transmission (%)
100
50
HO-2-/-
L-PAG
P=.017
I/O Ratio (A.U.)
1.0
0.5
HO-2-/-
L-PAG
C.
HO-2-/-
L-PAG
XIIn
∫preBötC
transmission failure
transmission failure
D.
HO-2-/-
L-PAG
XIIn
∫preBötC
E.
P=.045
Inspiratory Drive (pA)
0
-500
HO-2-/-
L-PAG